Research Square

Preprints are preliminary reports that have not undergone peer review.
They should not be considered conclusive, used to inform clinical practice,
or referenced by the media as validated information.

Pressure-Modulated Electroosmosis in pH-Responsive Zwitterionic Soft Nanochannels: Power-Law Fluid Study with Ion Steric and Partitioning Effects

Amit Malick

mantumalick94@gmail.com

IIMT University

Research Article

Keywords:

Posted Date: November 23rd, 2026

DOI: https://doi.org/10.21203/rs.3.rs-11535721/v1

License: This work is licensed under a Creative Commons Attribution 4.0 International License.
Read Full License

Additional Declarations: No competing interests reported.

Pressure-Modulated Electroosmosis in pH-Responsive Zwitterionic Soft Nanochannels: Power-Law Fluid Study with Ion Steric and Partitioning Effects

Amit Malick[a*]

[a]Department of Basic Science, School of Sciences, IIMT University, Meerut-250001, India

Abstract

This work extends a previously established self-consistent model of electroosmotic flow in zwitterionic soft nanochannels by incorporating an external pressure gradient into the original electric-field-driven formulation. Rather than assuming a fixed charge density, the charge of the polyelectrolyte layer is determined self-consistently through an acid–base equilibrium that depends on the local hydrogen-ion concentration and electric potential, leading to charge reversal at the isoelectric point ($\mathrm{pH} \approx 6.6$). The governing equations couple the momentum equation, augmented by a pressure-driven body force, with a modified Poisson–Boltzmann equation that incorporates finite ion-size effects through Carnahan–Starling theory and ion solvation through the Born energy, together with a drag force arising from the grafted polymer chains. The coupled nonlinear equations are solved numerically and validated against the Debye–Hückel limit. Since the pressure gradient appears only in the momentum equation, it does not alter the electric potential distribution or the isoelectric pH. However, it shifts the pH corresponding to flow reversal and introduces an approximately uniform offset in the velocity variations caused by ion size and electrolyte concentration, while leaving ion selectivity nearly unchanged because its convective contribution affects cations and anions equally. Shear-thinning fluids achieve velocities up to four times greater than those of Newtonian fluids, whereas increasing ion size suppresses the flow owing to enhanced steric exclusion. Overall, the results demonstrate that the external pressure gradient serves as an independent control parameter capable of accelerating, decelerating, or even reversing pH-regulated electroosmotic flow without significantly affecting the chemically governed ion selectivity.

Keywords: Electroosmotic flow, Pressure-driven flow, Power-law fluid, pH-regulated nanochannel, Soft nanochannel, Ion steric effects, Ion partitioning, Polyelectrolyte layer

*Corresponding author. E-mail: amitmalick_sobst@iimtu.edu.in, Telephone: +91-9064307911

Nomenclature

Symbol	Description (units)
h	channel half-height (m)
$\delta,\ \bar{\delta} = \delta/h$	PEL thickness (m), dimensionless form
E_0	axial electric field (V/m)
n_0	bulk electrolyte concentration (mM)
z	electrolyte valence
F	Faraday constant (C/mol)
$\epsilon_f,\ \epsilon_p$	electrolyte, PEL permittivity (F/m)
$\epsilon_r = \epsilon_p/\epsilon_f$	permittivity (ion-partition) ratio
r	hydrated ion radius (m)
ϕ_B	bulk ion volume fraction
P	ion-steric packing parameter
f	ion-partitioning coefficient
$k_B,\ T$	Boltzmann constant, temperature
e	elementary charge (C)
N_{Av}	Avogadro's number (1/mol)
$\psi,\ \bar{\psi} = \psi/\phi_0$	potential, dimensionless potential
$\phi_0 = k_B T/ze$	thermal potential scale (V)
$\kappa,\ \kappa h$	inverse Debye length (1/m), Debye–Hückel parameter
$\mathrm{p}K_a,\ \mathrm{p}K_b$	dissociation constants of acidic and basic groups
$N_A,\ N_B$	acidic and basic site densities (mM)
ρ_{fix}	PEL fixed-charge density (C/m^3)
$\mathrm{pH}_{\mathrm{iep}}$	isoelectric pH of the PEL
$u,\ \bar{u} = u/U^N_{\mathrm{HS}}$	axial velocity (m/s), dimensionless form
U^N_{HS}	Helmholtz–Smoluchowski velocity scale (m/s)
$m,\ n$	consistency index (Pa·s^n), flow behaviour index
$dp/dx,\ \Gamma$	axial pressure gradient (Pa/m), dimensionless pressure-gradient parameter
ϵ	PEL porosity
$K^*,\ \mu^*$	modified PEL permeability (m^{n+1}), consistency index
β	PEL softness parameter
$I_c,\ I_a,\ S$	cation/anion current, ion selectivity
$y,\ \bar{y} = y/h$	transverse coordinate, dimensionless form

1 Introduction

Polymer chains attached to a channel wall can respond to their surrounding chemical environment, whereas a bare, rigid wall cannot. When the pH varies, the functional groups on the chains accept or release protons, and when the salt concentration changes, the chains expand or contract. Soft nanochannels lined with a polyelectrolyte layer (PEL), rather than a bare charged wall, have become a natural platform for nanofluidic devices that require more than the simple passage of fluid through a narrow opening [20, 41, 45, 46, 1]. Biological systems already exploit this responsiveness: proteins, DNA, and zwitterionic polymers all possess ionisable groups whose charge state responds to the local pH [42, 63, 13]. A PEL-coated channel is, in essence, a synthetic analogue of this mechanism for applications such as chemical analysis [47], energy conversion [53,23,58], lab-on-a-chip systems [22,64,54], and biological diagnostics [17].

Fluid is moved through such a channel by two mechanisms. Pressure-driven flow (PDF) [57,65,56] is driven by an externally imposed pressure gradient, whereas electroosmotic flow (EOF) [49,8,32] is driven by an applied electric field that acts on the electric double layer (EDL) formed wherever a charged surface meets an electrolyte. A tangential electric field drags the charged layer and the bulk liquid along the channel [27, 24,38]. In a soft nanochannel, the diffuse, ion-permeable PEL, rather than a sharp interface, is the relevant "surface," and a body of research over the past two decades has shown how the characteristics of this layer influence the EOF response. Electroosmotic flow can be dramatically changed by the density and conformation of grafted polymer chains close to a charged surface, as first demonstrated by Harden et al. [25]. This idea has since been extended in several directions: Li et al. [31] examined how DNA type, incubation time, and ionic concentration affect the EOF velocity in DNA-modified channels; Bag et al. [3] directly connected the charge pattern within the polyelectrolyte layer (PEL) to ion selectivity; and Cao et al. [10] used coarse-grained molecular dynamics methods to understand the nature of EOF in polymer-brush-grafted channels at the molecular scale. Together, these studies showed that the extent to which a channel permits the flow of one ionic species relative to another depends not only on the geometric structure of the layer but also on its chemical nature. Closer to the present problem, Sadeghi et al. [51] and Chen et al. [13] each developed theoretical frameworks in which the PEL charge itself responds to pH and reported that pH, salt concentration, and channel geometry jointly control the transport behaviour. Related results for EOF in soft nanochannels appear in [29,61,37,43,7,60,12]. Thermal aspects of this same coupled EOF–PDF problem have also received attention. Matin et al. [39,40] examined how the governing parameters affect the Nusselt number in combined EOF–PDF through soft channels, Sarkar et al. [52] investigated the magnetohydrodynamic case, and Zhao et al. [68] incorporated ion partitioning into the thermal problem. In all of these studies, however, the working fluid was Newtonian.

This last restriction matters because most fluids of practical interest, such as blood, polymer solutions, and many other biological fluids, are not Newtonian. Their shear stress and shear rate are related nonlinearly, which rules out the ordinary Navier–Stokes equations and calls instead for the more general Cauchy

momentum balance. Once that step is taken, a choice of rheological model is still needed, and several have been tried: the Carreau model [70], the Maxwell model [28], the Herschel–Bulkley model [26,9], the Casson model [50], and the Jeffrey model [33], following the early analyses of Das et al. [16] and Chakraborty [11]. The power-law model has proved the most durable of these, largely because it captures shear-thinning and shear-thickening behaviour with a single exponent while remaining tractable enough for the EDL coupling to stay analytically or semi-analytically manageable. Zhao et al. [67,66] obtained a generalised Smoluchowski velocity relation valid for both Newtonian and power-law fluids and showed, perhaps counter-intuitively, that the wall shear stress does not depend on the power-law index; Vasu et al. [59] and Choi et al. [14] extended the high-zeta-potential regime; and Banos et al. [5] found that shear-thinning fluids carry species more efficiently than Newtonian ones under oscillatory EOF, with wall slip playing a non-trivial role. Deng et al. [18] and Babaie et al. [2] extended the power-law treatment to, respectively, transient two-layer heat transfer and combined pressure-driven/electroosmotic flow.

A separate thread of the literature has chipped away at a different simplification: the assumption that ions are dimensionless point charges. Real ions occupy volume, and once the PEL charge or the electrolyte concentration is large enough, that finite size measurably reshapes both the EDL potential and the resulting flow. A second, related correction is ion partitioning, which appears whenever the PEL and the bulk electrolyte differ in dielectric permittivity, since an ion crossing that interface then faces a Born energy penalty. For Newtonian fluids, the consequences of these two corrections are fairly well documented. Storey et al. [55] showed that the classical Poisson–Boltzmann equation breaks down at high frequency precisely because it ignores ion size, and argued for a mean-field correction such as the Carnahan–Starling model; this is the correction we adopt below. Liu et al. [34], Zheng et al. [69], Bandopadhyay et al. [4], Dey et al. [19], and Xing et al. [62] have each, in different geometries and under different combinations of wall slip and surface charge, traced how finite ion size and ion partitioning reshape entropy generation, electroosmotic thrust, size-selective transport, heat transfer, and mixed EOF–PDF flow.

For non-Newtonian fluids, the corresponding picture is considerably sparser. Paul et al. [44] looked at how ion partitioning alters electrokinetic transport of non-Newtonian fluids in PEL-coated channels, and Fadaei et al. [21] added finite ion size to a thermal EOF–PDF problem in a microchannel; beyond these two studies, the combination of power-law rheology with both steric and partitioning corrections together is largely unexplored. We closed part of this gap in earlier work: Malick and Barman [36] built a model that couples a modified Poisson–Boltzmann equation, incorporating both the Carnahan–Starling steric correction and Born-energy partitioning, to the Cauchy momentum and Brinkman equations for a power-law fluid in a soft nanochannel. That model showed clearly how steric and partitioning effects jointly shape EOF and ion selectivity, but it carried one structural limitation: the PEL charge density N was written into the model as a fixed, externally imposed constant. Real PELs, however, are rarely chemically inert in this way; if the grafted layer carries acidic or basic functional groups, its charge is not a parameter one chooses, but

a quantity the local pH determines through ordinary acid–base equilibrium. A constant-charge model has nothing to say about what happens as that pH is varied, including the qualitatively distinct regime where the PEL's net charge changes sign altogether.

The current investigation begins with this distinction. We allow the PEL to arise from the protonation and deprotonation equilibria of a zwitterionic layer containing both acidic (AH) and basic (B) radicals, rather than prescribing its charge value in advance. As a result, instead of having a fixed value, the fixed charge density ρ_{fix} becomes a function of the bulk pH and the local potential ψ. This self-consistent, pH-dependent description of the zwitterionic charge was recently developed and validated by us for a nanochannel driven solely by an electric field [35], where we showed that the net PEL charge and the EOF direction reverse at the isoelectric point, and that, once κh exceeds about 20, the ion-selectivity mechanism shifts from electrostatic to kinetic control, governed primarily by the relative mobilities of the background K^+ and Cl^- ions. The present paper keeps that electrostatic description intact and asks a different question: what happens when a mechanical pressure gradient is superimposed on this electrochemically gated flow? We show below that, because the pressure term enters only the momentum balance and never the electrostatics, the isoelectric point and the underlying charge-reversal mechanism established in [35] are left completely untouched by pressure; what changes is where the *flow* itself reverses and how strongly the ion current responds. The remainder of the paper develops the combined EOF–PDF momentum model, and then examines, largely through this pressure-electrostatics decoupling, how the flow-reversal point, the velocity field, and the ion selectivity of the channel respond to the pressure-gradient parameter Γ once it is added to the already-established pH-, ion-size-, and partitioning-dependent picture.

2 Problem Formulation and Mathematical Model

2.1 Model Description and Physical Configuration

Consider a symmetric soft nanochannel with a half-height of h, coated with a pH-sensitive polyelectrolyte layer (PEL) of uniform thickness (δ) on the channel walls. The PEL comprises zwitterionic functional groups that include both acidic (AH) and basic (B) moieties, and their ionisation states change depending on the local pH and electrostatic potential. The channel contains a symmetric binary electrolyte with an ionic valence of z and a bulk concentration of n_0. Electroosmotic flow is driven by an axial electric field of magnitude E_0, while pressure-driven flow arises from an applied pressure gradient dp/dx. The flow is assumed to be unidirectional, fully developed, and steady. Due to symmetry around the channel centreline, only the upper half of the channel ($0 \leq y \leq h$) is considered.

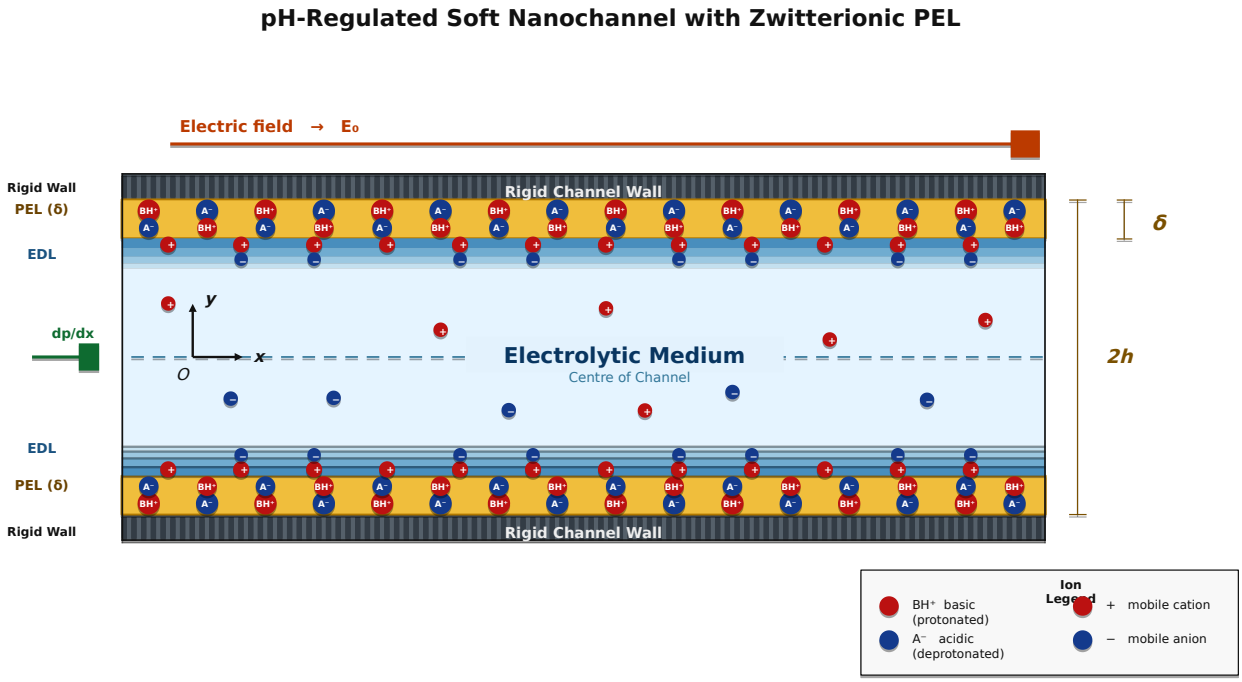


Figure 1: Schematic of combined EOF and PDF in a pH-regulated soft nanochannel. The PEL of thickness δ is attached to the upper channel wall; only the upper half ($0 \leq y \leq h$) is shown, owing to symmetry.

The electrokinetic response of this system is governed by three characteristic length scales: the channel half-height h, the Debye screening length κ^{-1}, and the ion radius r, which represents the finite size of the ions. The interplay among these parameters governs the degree of electric double layer (EDL) overlap, steric exclusion, and the overall transport characteristics. The underlying physical mechanism is determined by

the interaction of four effects. Electrostatic interactions are characterised by the electrokinetic parameter κh, where $\kappa = \sqrt{2z^2F^2n_0/(\epsilon_f RT)}$ is the inverse Debye length. Steric confinement is characterised by the bulk ion volume fraction $\phi_B = (4\pi r^3/3)(2n_0 N_{\mathrm{Av}})$, where r is the ion radius and N_{Av} is Avogadro's number. Chemical control is characterised by the bulk pH relative to the dissociation constants $\mathrm{p}K_a$ and $\mathrm{p}K_b$. The power-law index n characterises the rheological response, distinguishing shear-thinning ($n < 1$), Newtonian ($n = 1$), and shear-thickening ($n > 1$) behaviour. Together, these four effects govern the electrokinetic and transport characteristics of the system.

2.2 pH-Regulated Charge Density via Chemical Equilibrium

The self-consistent description of the PEL charge is an important aspect of this model, and reproduces for completeness the acid–base equilibrium framework we validated separately for the pure-EOF case in [35]; it is restated here because Section 2.5 couples it to a pressure-driven momentum balance that was absent from that earlier study. Rather than prescribing the charge density, we base it on the thermodynamic equilibrium of the protonation/deprotonation reactions. The dissociation of the acidic group AH follows the reaction $\mathrm{AH} \rightleftharpoons \mathrm{A}^- + \mathrm{H}^+$ (dissociation constant K_a), while the protonation of the basic group B follows the reaction $\mathrm{B} + \mathrm{H}^+ \rightleftharpoons \mathrm{BH}^+$ (association constant K_b). The law of mass action determines the fraction of charged sites, but the formula is modified to account for the electrostatic work required to bring a charge to the local potential ψ. This gives the following expressions for the occupation probabilities:

$$\mathcal{F}_A = \frac{1}{1 + 10^{\mathrm{p}K_a - \mathrm{pH}} \exp\left(-\dfrac{e\psi}{k_B T}\right)}, \tag{1a}$$

$$\mathcal{F}_B = \frac{1}{1 + 10^{\mathrm{pH} - \mathrm{p}K_b} \exp\left(+\dfrac{e\psi}{k_B T}\right)}. \tag{1b}$$

The net volumetric fixed charge density is then

$$\rho_{\mathrm{fix}}(\psi, \mathrm{pH}) = F\left[z_A N_A \mathcal{F}_A + z_B N_B \mathcal{F}_B\right], \tag{2}$$

Here, z_A and z_B are the valencies of the ionised groups (usually $z_A = -1$ and $z_B = +1$), and N_A and N_B are the total site densities of the acidic and basic groups, respectively. This configuration produces a crucial feedback loop: the potential ψ influences the charge density through the exponential terms, and the charge density, in turn, affects the potential through the Poisson equation. In the fixed-charge model of [36], only one term dominates, and the exponential dependence on ψ is neglected.

Eq. (2) leads to charge reversal. The net charge changes sign when the contributions from the two groups balance, that is,

$$z_A N_A \mathcal{F}_A + z_B N_B \mathcal{F}_B = 0. \tag{3}$$

This condition indirectly specifies the $\mathrm{pH}_{\mathrm{iep}}$ (isoelectric point) through Eq. (3). Because both $\mathcal{F}_A$ and $\mathcal{F}_B$ depend on ψ, the $\mathrm{pH}_{\mathrm{iep}}$ is not a fixed material constant; rather, its value changes with the local electrostatic environment. For equal site densities ($N_A = N_B$) and opposite unit valencies ($z_A = -1$, $z_B = +1$), the equilibrium condition is $\mathcal{F}_A = \mathcal{F}_B$. An explicit solution can be obtained by cross-multiplying and taking the $\log_{10}$ of both sides:

$$\mathrm{pH}_{\mathrm{iep}}(\psi) = \frac{\mathrm{p}K_a + \mathrm{p}K_b}{2} - \frac{e\psi}{2.303\, k_B T}, \tag{4}$$

which is independent of the (common) site density. A key qualitative finding of this study is illustrated by Eq. (4), which shows that the pH at which the PEL is electrically neutral varies linearly with the local potential ψ about the midpoint of the two dissociation constants. This behaviour is not seen in the fixed-charge model, where the sign of the total charge becomes fixed once the value of N is set. For unequal site densities, the equilibrium condition can no longer be reduced to a simple logarithmic form; instead, $\mathrm{pH}_{\mathrm{iep}}$ is found as the physical root of a quadratic equation in 10^{pH}, a result we have derived using the other system parameters, though the details are not given here.

2.3 Modified Poisson–Boltzmann Equation with Steric and Partitioning Corrections

The electrostatic potential satisfies Poisson's equation in each region:

$$-\frac{d}{dy}\left[\epsilon(y)\frac{d\psi}{dy}\right] = \rho(y), \tag{5}$$

where $\epsilon(y) = \epsilon_f$ in the electrolyte region ($0 \le y \le h - \delta$) and $\epsilon(y) = \epsilon_p < \epsilon_f$ in the PEL ($h - \delta \le y \le h$). The total charge density is

$$\rho(y) = \begin{cases} \rho_e(\psi), & 0 \le y \le h - \delta, \\ f\,\rho_e(\psi) + \rho_{\mathrm{fix}}(\psi, \mathrm{pH}), & h - \delta \le y \le h, \end{cases} \tag{6}$$

where $\rho_e = zF(n_c - n_a)$ is the mobile charge density and f is a partitioning coefficient that discounts the mobile-ion contribution inside the lower-permittivity PEL. The mobile ion concentrations incorporate finite-size (steric) effects through a modified Boltzmann distribution,

$$n_{c,a}(y) = \frac{\gamma^{\infty}}{\gamma(y)}\, n_0 \exp\left(\mp \frac{ze\psi}{k_B T}\right), \tag{7}$$

where $\gamma(y)$ and γ^{∞} are, respectively, the local and bulk ionic activity coefficients. The Carnahan–Starling equation of state for the hard-sphere ion fluid provides an explicit estimate for the activity ratio in terms of the bulk volume fraction ϕ_B.

$$\frac{\gamma^{\infty}}{\gamma(y)} = \frac{1}{1 + P\left[\cosh\left(\dfrac{ze\psi}{k_B T}\right) - 1\right]}, \qquad P = \frac{8\phi_B}{1 + 8\phi_B}. \tag{8}$$

The partitioning coefficient f arises from the Born self-energy cost an ion pays when it moves from the electrolyte, of permittivity ϵ_f, into the lower-permittivity PEL:

$$f = \exp\left[-\frac{(ze)^2}{8\pi r k_B T}\left(\frac{1}{\epsilon_p} - \frac{1}{\epsilon_f}\right)\right]. \tag{9}$$

The modified Poisson–Boltzmann equation is obtained by substituting the charge density of Eq. (6), together with the mobile charge density $\rho_e = -2zFn_0\,(\gamma^{\infty}/\gamma)\sinh(ze\psi/k_BT)$ obtained from Eq. (7), into Poisson's equation, Eq. (5).

$$\frac{d^2\psi}{dy^2} = \begin{cases} \dfrac{2zFn_0}{\epsilon_f}\,\dfrac{\gamma^{\infty}}{\gamma(y)}\sinh\left(\dfrac{ze\psi}{k_BT}\right), & 0 \le y \le h - \delta, \\[2ex] \dfrac{2zFn_0 f}{\epsilon_p}\,\dfrac{\gamma^{\infty}}{\gamma(y)}\sinh\left(\dfrac{ze\psi}{k_BT}\right) - \dfrac{\rho_{\text{fix}}(\psi, \text{pH})}{\epsilon_p}, & h - \delta \le y \le h. \end{cases} \tag{10}$$

In contrast to the constant-charge model, Eq. (10) is essentially nonlinear because the fixed charge ρ_{fix} that generates the potential is itself a function of that potential through Eq. (2). Consequently, the values of ψ and ρ_{fix} must be determined self-consistently rather than sequentially.

2.4 Dimensionless Electrostatic System

To cast Eq. (10) into the form required by the finite-difference scheme of Section 2.7, we scale lengths by the channel half-height, $\bar{y} = y/h$ and $\bar{\delta} = \delta/h$, and the potential by the thermal voltage $\phi_0 = k_BT/(ze)$, so that $\bar{\psi} = \psi/\phi_0 = ze\psi/(k_BT)$ measures the potential in units of k_BT/e. Under this scaling, and with $\kappa^2 = 2zFn_0/(\epsilon_f\phi_0) = 2z^2F^2n_0/(\epsilon_f RT)$ the Debye parameter already introduced in Section 2.1 and $\epsilon_r = \epsilon_p/\epsilon_f$, Eq. (10) becomes

$$\frac{d^2\bar{\psi}}{d\bar{y}^2} = \begin{cases} (\kappa h)^2\,\dfrac{\sinh(\bar{\psi})}{1 + P[\cosh(\bar{\psi}) - 1]}, & 0 \le \bar{y} \le 1 - \bar{\delta}, \\[2ex] \dfrac{(\kappa h)^2}{\epsilon_r}\left[\dfrac{f\sinh(\bar{\psi})}{1 + P[\cosh(\bar{\psi}) - 1]} - \bar{Q}_{\text{fix}}(\bar{\psi}, \text{pH})\right], & 1 - \bar{\delta} \le \bar{y} \le 1, \end{cases} \tag{11}$$

where the dimensionless fixed charge is

$$\bar{Q}_{\text{fix}}(\bar{\psi}, \text{pH}) = \frac{z_A\bar{N}_A}{1 + 10^{\text{p}K_a - \text{pH}}e^{-\bar{\psi}}} + \frac{z_B\bar{N}_B}{1 + 10^{\text{pH} - \text{p}K_b}e^{+\bar{\psi}}}, \qquad \bar{N}_{A,B} = \frac{N_{A,B}}{2n_0 z}. \tag{12}$$

The grouping κh is the Debye–Hückel parameter, the ratio of the channel half-height to the EDL thickness; it tells us whether the EDLs of the two walls overlap (κh small) or stay well separated (κh large). The

isoelectric-point condition of Eq. (4) carries through this rescaling unchanged, since $\bar{Q}_{\text{fix}} = 0$ at exactly the same pH as $\rho_{\text{fix}} = 0$.

The boundary conditions on $\bar{\psi}$ are

$$\begin{cases} \left.\dfrac{d\bar{\psi}}{d\bar{y}}\right|_{\bar{y}=0} = 0, \\ \bar{\psi}\big|_{\bar{y}=(1-\bar{\delta})^-} = \bar{\psi}\big|_{\bar{y}=(1-\bar{\delta})^+}, \\ \left.\dfrac{d\bar{\psi}}{d\bar{y}}\right|_{\bar{y}=(1-\bar{\delta})^+} = \epsilon_r \left.\dfrac{d\bar{\psi}}{d\bar{y}}\right|_{\bar{y}=(1-\bar{\delta})^-}, \\ \left.\dfrac{d\bar{\psi}}{d\bar{y}}\right|_{\bar{y}=1} = 0. \end{cases} \tag{13}$$

The first condition expresses symmetry about the channel centreline, the second and third express continuity of potential and normal electric displacement across the PEL interface, and the fourth expresses the absence of any additional surface charge at the outer wall beyond what is already carried by ρ_{fix}.

2.5 Momentum Transport and Rheology

The axial velocity $u(y)$ satisfies a generalised Cauchy–Brinkman equation, obtained from the axial component of the momentum balance together with a Darcy-type drag term representing the resistance of the grafted polymer segments inside the PEL:

$$\rho_f \frac{Du}{Dt} = -\frac{dp}{dx} + \frac{d\tau_{xy}}{dy} + \rho_e E_0, \qquad 0 \le y \le h - \delta, \tag{14a}$$

$$\rho_f \frac{Du}{Dt} = -\frac{dp}{dx} + \frac{d\tau_{xy}}{dy} + f\rho_e E_0 + \rho_{\text{fix}} E_0 - \frac{\mu^*}{K^*}\, u|u|^{n-1}, \qquad h - \delta \le y \le h, \tag{14b}$$

subject everywhere to incompressibility. The body-force terms $\rho_e E_0$ and $(f\rho_e + \rho_{\text{fix}})E_0$ are precisely the electrostatic charge densities of Section 2.3, now acting as the electroosmotic driving force; this is the explicit link between the electrostatics developed above and the flow field solved below.

For the steady, fully developed, unidirectional flow considered here, inertial terms vanish identically and the shear stress follows the power-law constitutive relation

$$\tau_{xy} = m \left|\frac{du}{dy}\right|^{n-1} \frac{du}{dy}, \tag{15}$$

with m the flow consistency index and n the power-law index: $n < 1$ describes a shear-thinning fluid, $n > 1$ a shear-thickening fluid, and $n = 1$ recovers the Newtonian case. The permeability of the PEL to a power-law fluid, adapted from the classical Blake–Kozeny-type result for power-law flow through a packed bed of spheres derived by Christopher and Middleman [15], is

$$K^* = \frac{6}{25}\left(\frac{n\epsilon}{3n+1}\right)^n \left(\frac{\epsilon d_s}{3(1-\epsilon)}\right)^{n+1}, \qquad \mu^* = m\epsilon^n, \tag{16}$$

with ϵ the porosity of the grafted layer and d_s the diameter of an individual polymer segment.

Scaling the velocity by the generalised Helmholtz–Smoluchowski velocity $U_{\mathrm{HS}}^N = n\kappa^{(1-n)/n}(\epsilon_f E_0 \psi_0/m)^{1/n}$ and defining $\bar{u} = u/U_{\mathrm{HS}}^N$, substitution of Eq. (15) into Eqs. (14a)–(14b) gives the dimensionless momentum equation:

$$\frac{d}{d\bar{y}}\left[\left|\frac{d\bar{u}}{d\bar{y}}\right|^{n-1}\frac{d\bar{u}}{d\bar{y}}\right] = \begin{cases} -\dfrac{(\kappa h)^{n-1}}{n^n}\,2\Gamma + \dfrac{(\kappa h)^{n-1}}{n^n}\dfrac{d^2\bar{\psi}}{d\bar{y}^2}, & 0 \le \bar{y} \le 1-\bar{\delta}, \\ -\dfrac{(\kappa h)^{n-1}}{n^n}\,2\Gamma + \dfrac{\epsilon_r(\kappa h)^{n-1}}{n^n}\dfrac{d^2\bar{\psi}}{d\bar{y}^2} + \beta^2\,\bar{u}|\bar{u}|^{n-1}, & 1-\bar{\delta} \le \bar{y} \le 1, \end{cases} \tag{17}$$

where the pressure-gradient parameter and softness parameter are, respectively,

$$\Gamma = -\frac{h^2}{2m}\frac{dp}{dx}, \qquad \beta = \frac{h^{(n+1)/2}}{\sqrt{K^*/\epsilon^n}}. \tag{18}$$

$\Gamma > 0$ corresponds to a pressure gradient that assists the electroosmotic flow and $\Gamma < 0$ to one that opposes it; β grows as the PEL becomes more densely grafted and therefore more resistive, and typically ranges from 1 to 100 for PELs of practical interest.

The boundary conditions on $\bar{u}$ are

$$\begin{cases} \bar{u}\big|_{\bar{y}=1} = 0 \quad \text{(no-slip at wall)}, \\ \bar{u}\big|_{\bar{y}=(1-\bar{\delta})^-} = \bar{u}\big|_{\bar{y}=(1-\bar{\delta})^+} \quad \text{(velocity continuity)}, \\ \left.\dfrac{d\bar{u}}{d\bar{y}}\right|_{\bar{y}=(1-\bar{\delta})^-} = \left.\dfrac{d\bar{u}}{d\bar{y}}\right|_{\bar{y}=(1-\bar{\delta})^+} \quad \text{(shear stress continuity)}, \\ \left.\dfrac{d\bar{u}}{d\bar{y}}\right|_{\bar{y}=0} = 0 \quad \text{(symmetry condition)}. \end{cases} \tag{19}$$

2.6 Ionic Selectivity and the Charge-Reversal Signature

The selective transport of ions through the channel is quantified by the selectivity parameter S, defined in terms of the cross-sectionally averaged cation current I_c (the current carried by K^+) and the cross-sectionally averaged anion current I_a (the current carried by Cl^-) as

$$S = \frac{|\langle I_c\rangle| - |\langle I_a\rangle|}{|\langle I_c\rangle| + |\langle I_a\rangle|}, \tag{20}$$

where the cross-sectionally averaged current of ionic species i, combining diffusive, convective, and electromigrative contributions, is

$$\langle I_i \rangle = \frac{1}{h} \int_0^h \left[-D_i \frac{dn_i}{dy} + u(y)\, n_i(y) + \frac{z_i e D_i}{k_B T}\, n_i(y)\, E_0 \right] dy. \tag{21}$$

The charge-reversal term in equation (4) indicates that the sign of S changes when the bulk pH exceeds $\mathrm{pH}_{\mathrm{iep}}$. At that point, the overall charge of the PEL, and hence the nature of the Donnan exclusion between cations and anions, reverses, and the selectivity changes accordingly. This sign reversal is a direct result of the pH-controlled charging mechanism described earlier; it has no counterpart in the fixed-charge model, in which S always favours a certain ionic species for a given PEL. The interplay of pH, steric effects, ion partitioning, and rheology, which controls the extent and intensity of this transition or reversal, is examined numerically in Section 3.

2.7 Numerical Solution Procedure

The coupled system of equations (11) and (17), along with the boundary conditions (13) and (19), is numerically solved using a second-order central finite difference method on a uniform grid. The Tridiagonal Matrix Algorithm (TDMA) is used iteratively to resolve the nonlinearities, including Picard iteration for the modified Poisson–Boltzmann equation and Newton–Raphson linearisation for the power-law term in the momentum equation. Convergence is achieved when the maximum difference between successive iterations is less than 10^{-6}. Grid independence is demonstrated by comparing results from grids with 200, 400, and 800 nodes, and the numerical solutions are validated against the closed-form analytical solution obtained under the Debye–Hückel approximation with constant PEL charge density.

3 Results and Discussion

We analyse the influence of various parameters on the potential distribution and average axial velocity of a power-law fluid within pH-controlled, polymer-grafted soft nanochannels. The parameters involved in the potential and velocity equations include r (ion size), ϵ_r (the ratio of the permittivities of the electrolyte and the PEL, which governs the ion-partitioning effect), h (channel half-height), δ (PEL thickness), n (fluid behaviour index), and several others. The ranges of these parameters are selected based on their practical relevance to fluid flow in polymer-grafted nanochannels. Furthermore, they are aligned with the zwitterionic PEL chemistry employed in [35] to facilitate a direct comparison of results between the two studies. We assume a channel half-height of $h = 25$ nm, a PEL thickness of $\delta = 0.1\,h$, and KCl as the background electrolyte. As the bulk electrolyte concentration varies from 10^{-2} mM to 10^{2} mM, the Debye–Hückel parameter ranges from 1 to 100. The dielectric permittivity of the PEL is adjusted such that the ion-partitioning parameter [48,30] falls between 0.1 and 1. The bulk pH of the electrolyte medium is varied between 2 and 12. Here, since $\mathrm{p}K_a = 4.58$ and $\mathrm{p}K_b = 8.6$, the isoelectric point, $\mathrm{pH}_{\mathrm{iep}}$, is approximately 6.59, and the flexibility parameter β varies between 1 and 10.

It is worth noting at the outset that Γ appears only in the momentum equation, Eq. (17), and not in the electrostatic system, Eq. (11). The EDL potential, fixed-charge density, and consequently $\mathrm{pH_{iep}}$, are determined solely by pH, ion size, and permittivity, and are therefore identical to those in the pure EOF case reported in [35], regardless of Γ. Since the role of the relative permittivity ϵ_r in the electrostatic system was already detailed there, we fix $\epsilon_r = 0.2$ and instead dedicate the parameter study to Γ, which effectively introduces a new degree of freedom into the existing model. The discussion proceeds as follows: we first briefly revisit the electrostatics to establish the baseline against which the pressure-modulated flow field is compared. We then focus on how superimposing Γ onto this fixed electrostatic backbone alters the velocity field, specifically examining the point at which the flow reverses direction and the ion-selectivity crossover shifts.

3.1 Baseline Electrostatics: The Γ-Independent EDL Potential

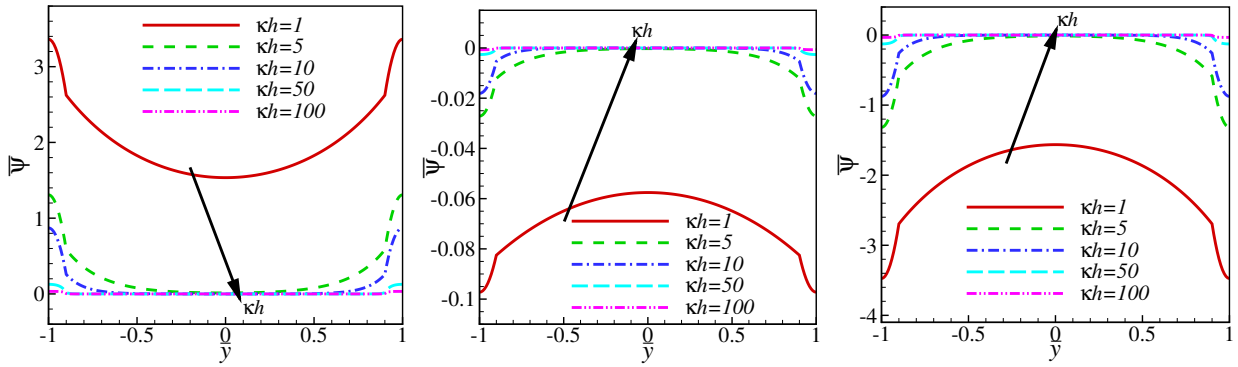


Figure 2: The potential distribution $\bar{\psi}(\bar{y})$ across the soft polymer-grafted nanochannel, shown as a function of the dimensionless transverse coordinate $\bar{y}$ for different values of $\kappa h = 1, 5, 10, 50, 100$ at fixed $\Gamma = -0.5$, for (a) pH $= 2$, (b) pH $= 7$, and (c) pH $= 12$. The value of κh increases in the direction of the arrow. The other model parameters are $z = 1$, $\epsilon_r = 0.2$, $N_A = N_B = 1$ mM, and $\beta = 1$.

Figures 2(a)–2(c) show the EDL potential distribution $\bar{\psi}(\bar{y})$ within the channel for various values of the Debye–Hückel parameter κh at three specific pH values; here, $\Gamma = -0.5$ is shown merely as a label for simplicity. Since Γ does not appear in equation (11), these profiles are identical for all values of Γ and accurately represent the pure EOF electrostatics described in [35]. In summary, increasing κh compresses the EDL and screens the PEL charge, causing the potential magnitude to decrease continuously across all pH values. Furthermore, the sign of $\bar{\psi}$ within the PEL depends on the protonation state of the zwitterionic groups: positive below the isoelectric point (Fig. 2(a)), near zero close to it (Fig. 2(b)), and negative above it (Fig. 2(c)). With this Γ-independent baseline established, the remainder of Section 3 examines how

superimposing the pressure-gradient parameter on this fixed electrostatic backbone reshapes the velocity field and ion selectivity.

3.2 Pressure-Modulated Velocity Field

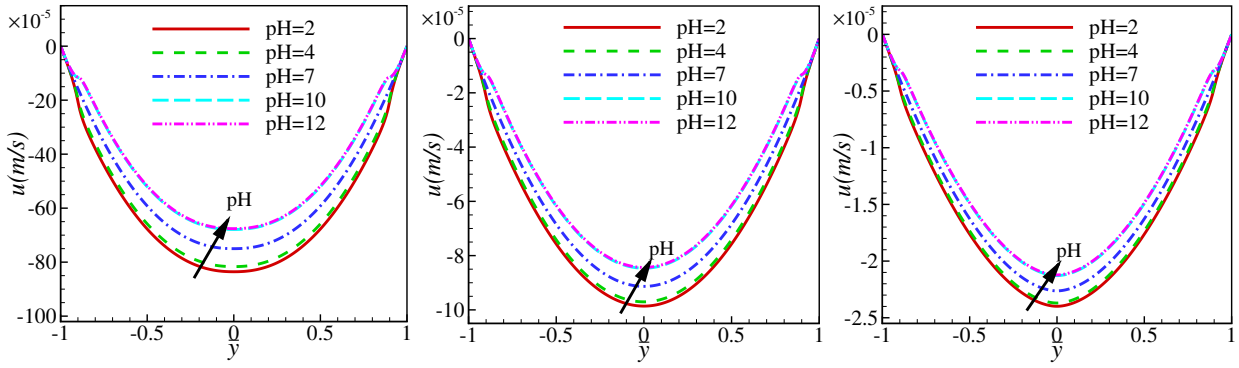
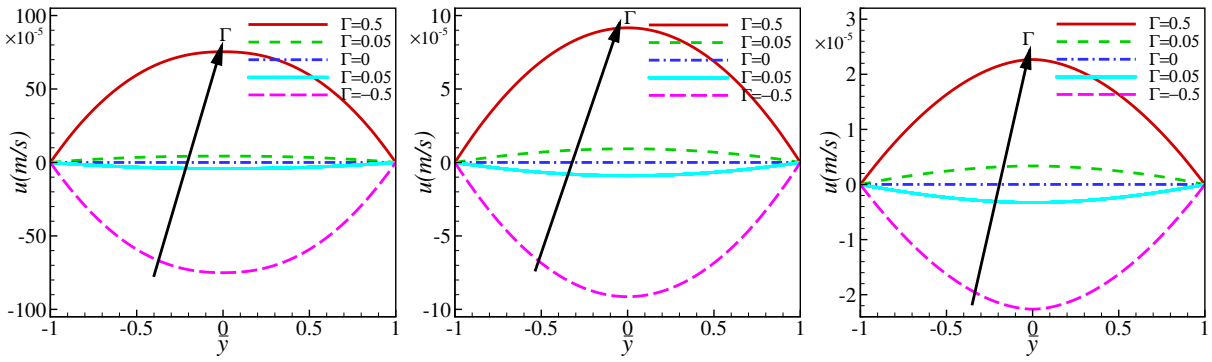


Figure 3: The mean axial velocity $\bar{u}(\bar{y})$ as a function of the transverse coordinate $\bar{y}$ in the soft polymer-grafted nanochannel for (a) $n = 0.8$, (b) $n = 1$, and (c) $n = 1.2$, with different values of $\mathrm{pH} = 2, 5, 7, 9, 12$ at a fixed adverse pressure gradient $\Gamma = -0.5$. The pH increases in the direction of the arrow. The other model parameters are $z = 1$, $\epsilon_r = 0.2$, $N_A = N_B = 1$ mM, $\kappa h = 50$, and $\beta = 1$.

Figures 3(a)–3(c) show how the velocity profile $\bar{u}(\bar{y})$ varies across the channel width under a fixed adverse pressure gradient $\Gamma = -0.5$. The pH-dependent charge-reversal process described earlier determines the direction of the electroosmotic driving force here, just as it does in pure EOF; however, in this case, the force is accompanied by a Poiseuille-type flow component due to the constant Γ. Consequently, these two components add at low pH and subtract at high pH (or vice versa, depending on the sign convention for Γ). As a result, the velocity is no longer zero at $\mathrm{pH}_{\mathrm{iep}}$, but rather at the pH value where these two components completely cancel each other; this is the flow-reversal point introduced earlier and analysed in greater detail in Figures 4 and 5.

The effect of the fluid behaviour index n is also clearly visible in these figures. In the shear-thinning case ($n = 0.8$), the velocity profile becomes more plug-like, with a steep gradient near the channel walls, whereas in the shear-thickening case ($n = 1.2$), the profile becomes more parabolic. This is consistent with previous studies on the electroosmotic flow of power-law fluids [67,2].



(a) (b) (c)

Figure 4: The mean axial velocity $\bar{u}(\bar{y})$ as a function of the transverse coordinate $\bar{y}$ in the soft polymer-grafted nanochannel for (a) $n = 0.8$, (b) $n = 1$, and (c) $n = 1.2$, with different values of the pressure-gradient parameter $\Gamma = -1, -0.5, 0, 0.5, 1$ at fixed pH $= 7$. The value of Γ increases in the direction of the arrow. The other model parameters are $z = 1$, $\epsilon_r = 0.2$, $N_A = N_B = 1$ mM, $\kappa h = 50$, and $\beta = 1$.

Figures 4(a)–4(c) show the mean axial velocity $\bar{u}(\bar{y})$ across the channel for different values of the pressure-gradient parameter Γ at a bulk pH of 7. As Γ changes from negative (adverse) to positive (favourable), the average flow velocity throughout the channel increases because the pressure-driven flow now adds to the electroosmotic transport rather than opposing it.

At pH 7, $\mathrm{p}K_a = 4.58 < 7 < \mathrm{p}K_b = 8.6$, the basic groups are primarily protonated (BH^+), whereas the acidic groups are generally undissociated. The PEL has a net positive fixed charge, resulting in a strong electroosmotic driving force even when there is no external pressure gradient ($\Gamma = 0$). A favourable pressure gradient ($\Gamma > 0$) accelerates the electroosmotic flow and increases its velocity, while an adverse pressure gradient ($\Gamma < 0$) slows the flow and decreases its velocity.

The fluid behaviour index n again plays a clear role, reproducing the same plug-like versus parabolic profile shapes noted for Fig. 3; the higher effective viscosity of the shear-thickening fluid keeps its profile closer to parabolic regardless of the sign or magnitude of Γ.

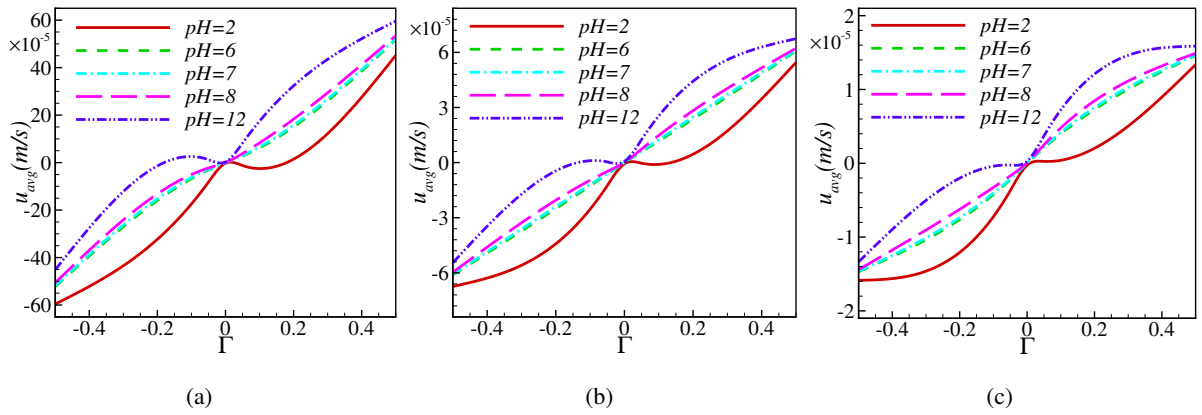


Figure 5: The average axial velocity $\bar{u}$ as a function of the dimensionless pressure-gradient parameter Γ in the soft polymer-grafted nanochannel for (a) $n = 0.8$, (b) $n = 1$, and (c) $n = 1.2$, with different values of pH $= 2, 5, 7, 9, 12$. The pH increases in the direction of the arrow. The other model parameters are $z = 1$, $\epsilon_r = 0.2$, $N_A = N_B = 1$ mM, $\kappa h = 50$, and $\beta = 1$.

Figures 5(a)–5(c) depict the average axial velocity as a function of the pressure-gradient parameter Γ at different bulk pH values. For a particular power-law index, the average velocity varies non-monotonically with pH because the ionisation of the acidic and basic groups within the zwitterionic PEL balances their respective effects. The velocity is notably high at highly acidic pH (net positive PEL charge, dominated by BH^+) and highly alkaline pH (net negative PEL charge, dominated by A^-), reaching a minimum near the isoelectric point, where the two contributions largely cancel each other. A shear-thinning fluid ($n = 0.8$) has the highest average velocity for a given Γ and pH, while a shear-thickening fluid ($n = 1.2$) has the lowest velocity, consistent with its greater effective viscosity. At the same pH and κh, the shear-thinning fluid exhibits a fourfold increase in average velocity compared to the Newtonian case, which aligns with the electroosmotic results presented in [35]. This illustrates that the rheological enhancement is not fundamentally affected by whether the flow is driven exclusively by an electric field or by both an electric field and a pressure gradient.

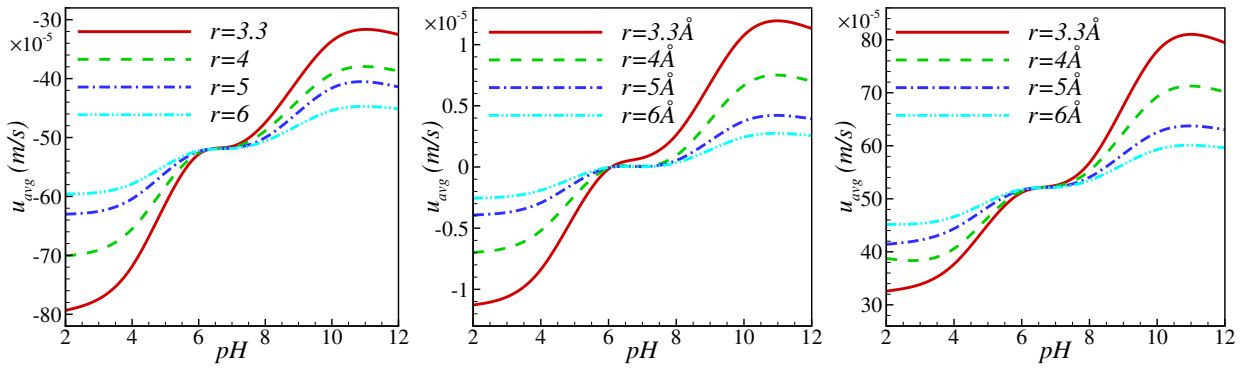


Figure 6: The average axial velocity $\bar{u}$ as a function of pH in the soft polymer-grafted nanochannel for $n = 0.8$ (shear-thinning fluid), with different values of ion radius $r = 3.3\,\text{Å},\ 4\,\text{Å},\ 5\,\text{Å},\ 6\,\text{Å}$, for (a) $\Gamma = -0.5$, (b) $\Gamma = 0$, and (c) $\Gamma = 0.5$. The ion radius r increases in the direction of the arrow. The other model parameters are $z = 1$, $\epsilon_r = 0.2$, $N_A = N_B = 1$ mM, $\kappa h = 50$, and $\beta = 1$.

Figures 6(a)–6(c) show the average axial velocity versus pH for a shear-thinning fluid ($n = 0.8$) under three different pressure-gradient values: $\Gamma = -0.5$ (adverse), $\Gamma = 0$ (pure EOF), and $\Gamma = 0.5$ (favourable). The middle panel ($\Gamma = 0$) replicates the steric-exclusion trend previously observed in [35]: larger ions at the PEL interface encounter a higher Born penalty, which compresses the effective counterion layer and uniformly reduces the velocity as r increases across all pH levels. The comparison among the three panels in Fig. 6 is a novel feature: the vertical offset resulting from $\Gamma \neq 0$ is independent of the value of r; therefore, favourable or adverse pressure gradients shift the entire velocity–pH curve upward or downward without changing the underlying steric-exclusion trend. This demonstrates that the steric and pressure-driven effects have separate and complementary roles in the flow.

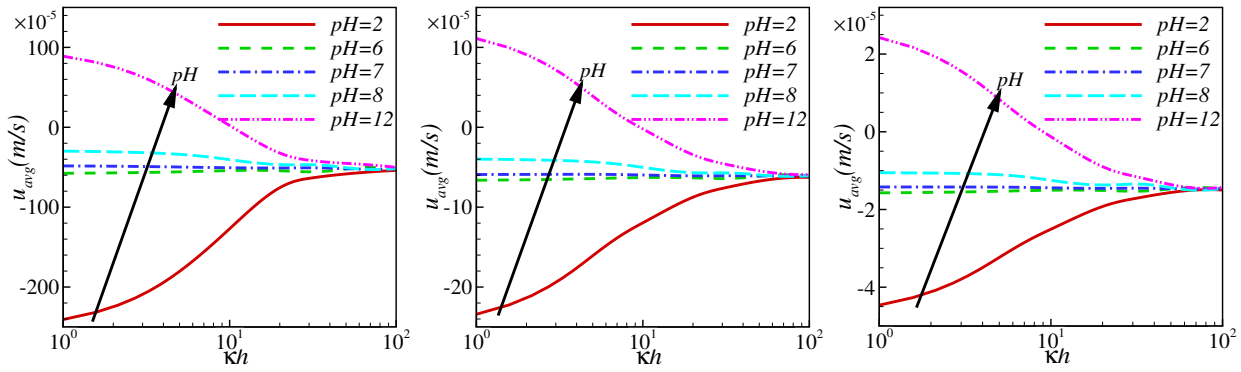


Figure 7: The average axial velocity $\bar{u}$ as a function of κh in the soft polymer-grafted nanochannel for $\Gamma = -0.5$ (pressure-opposed flow), with different values of bulk pH, $\mathrm{pH} = 2, 6, 7, 8, 12$, for (a) $n = 0.8$, (b) $n = 1$, and (c) $n = 1.2$. The bulk pH increases in the direction of the arrow. The other model parameters are $z = 1$, $\epsilon_r = 0.2$, $N_A = N_B = 1$ mM, and $\beta = 1$.

Figures 7(a)–7(c) illustrate the average axial velocity $\bar{u}$ as a function of the electrokinetic parameter κh for different bulk pH values, an adverse pressure gradient ($\Gamma = -0.5$), and three fluid behaviour indices. The velocity increases monotonically with κh and decreases monotonically with pH for every fluid behaviour index, the same qualitative dependence reported for the pure EOF channel in [35]. This trend persists even when the flow opposes an adverse pressure gradient, with the shear-thinning fluid remaining the fastest and the shear-thickening fluid the slowest throughout. This confirms that the adverse pressure offset does not alter the relative ranking determined by κh, pH, or n, but only their absolute magnitude.

3.3 Mobile Ion Selectivity

The selective transport of ions through a nanochannel is quantified by the selectivity parameter S. Here I_c denotes the cation (K^+) current and I_a the anion (Cl^-) current, each an average current density integrated throughout the channel cross-section [48,6], so that

$$S = \frac{|I_c| - |I_a|}{|I_c| + |I_a|}. \tag{22}$$

The parameter S lies within the interval $[-1, 1]$, where $S = 0$ denotes no net ionic selectivity, $S = -1$ denotes total anion selectivity, and $S = 1$ denotes complete cation selectivity (only cations are transported).

The sign and magnitude of S are determined by the same pH-dependent Donnan-exclusion mechanism described for pure EOF channels in [35]: the PEL is anion-selective ($S < 0$) below the isoelectric point and cation-selective ($S > 0$) above it, passing through $S \approx 0$ at $\mathrm{pH}_{\mathrm{iep}}$; furthermore, when κh becomes large enough to weaken electrostatic exclusion, the higher mobility of Cl^- relative to K^+ dominates, causing

the sign of S to flip even if the sign of the PEL charge remains unchanged. This behaviour persists here because, as discussed earlier, Γ does not alter the electrostatic exclusion mechanism. What Γ can do is affect the convective term $u(y)n_i(y)$ in Eq. (21), the only point at which the velocity field enters the ionic current expression. Since both ionic species are transported by the same $u(y)$, this convective contribution affects I_c and I_a in nearly the same way, thereby having a negligible impact on their difference, S, even though it may significantly alter the individual currents.

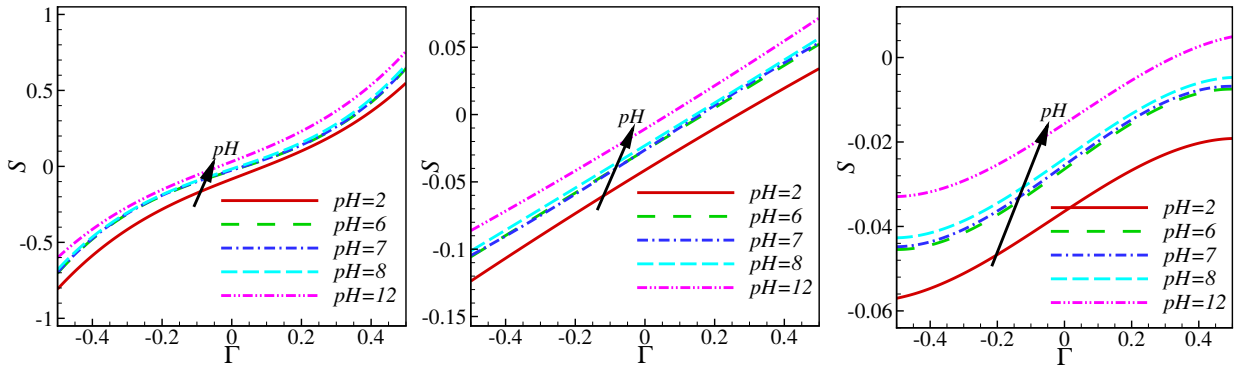


Figure 8: The selectivity parameter S as a function of the dimensionless pressure-gradient parameter Γ in the soft polymer-grafted nanochannel for (a) $n = 0.8$ (shear-thinning), (b) $n = 1$ (Newtonian), and (c) $n = 1.2$ (shear-thickening), with different values of bulk pH $= 2, 5, 7, 9, 12$. The pH increases in the direction of the arrow. The other model parameters are $z = 1$, $\epsilon_r = 0.2$, $N_A = N_B = 1$ mM, $\kappa h = 50$, and $\beta = 1$.

Figures 8(a)–8(c) show the selectivity parameter S as a function of Γ for three rheological conditions at different bulk pH values. Two aspects of this pressure-modulated behaviour are particularly noteworthy. At a given pH, $S(\Gamma)$ is essentially constant, which supports the quasi-symmetric convection argument. Varying Γ from -1 to 1 produces no change in the sign of S and only very minor variations in its magnitude; this contrasts with the effect of pH variation illustrated in Figs. 2–7, where the sign of S undergoes a substantial change. Second, the slight dependence on Γ varies with the fluid rheology: the magnitude $|S|$ is slightly higher for a shear-thinning fluid ($n = 0.8$) and slightly lower for a shear-thickening fluid ($n = 1.2$) than for a Newtonian fluid. This is because the convective term, which causes the small dependence of S on Γ, scales with $u(y)$, and the value of $u(y)$ is determined by n.

4 Conclusion

This study extends the self-consistent, pH-regulated zwitterionic charge model, which was previously explored and validated for pure EOF in [35], to soft nanochannels subjected to the simultaneous influence

of an axial electric field and an external pressure gradient. Instead of the fixed PEL charge used in our earlier fixed-charge study [36], a charge density derived self-consistently from acid–base equilibrium is employed here. The Carnahan–Starling steric correction, Born-energy-based ion partitioning, and power-law/Brinkman flow structure are maintained. A key structural finding is that the pressure-gradient parameter Γ appears only in the momentum balance equation; consequently, regardless of the value of Γ, the EDL potential, fixed-charge density, and isoelectric point ($\mathrm{pH_{iep}} \approx 6.59$) remain identical to those of the pure EOF channel described in [35]. Changing Γ modifies the flow field within this electrokinetic structure: it introduces an offset in the velocity–pH and velocity–κh plots that is essentially independent of ion size and fluid rheology, and it shifts the pH at which the mean velocity vanishes away from $\mathrm{pH_{iep}}$, without affecting the pH-dependent variation (Figs. 6 and 7). Ion selectivity is less sensitive than velocity to changes in Γ: the sign of S and the kinetic-controlled transition at $\kappa h > 20$ (described in [35]) remain essentially unchanged, with only minor variations in magnitude, as Γ is varied (Fig. 8). This is because Γ enters the ionic flux only through an advection term that is nearly identical for both ionic species. Both $\bar{u}$ and $|S|$ show non-monotonic behaviour with respect to pH, as in pure EOF; their values are lowest close to $\mathrm{pH_{iep}}$ and increase under highly acidic or alkaline conditions. When all other conditions are the same, a shear-thickening fluid has the lowest velocity, while a shear-thinning fluid ($n = 0.8$) has a velocity that is approximately four times that of a Newtonian fluid.

Overall, these findings show that the applied pressure gradient functions as an independent regulator in pH-controlled soft nanochannels: it can change the location and velocity of the flow-reversal point, but it has no effect on the chemical selectivity crossover that determines which ionic species the channel preferentially transports. The current framework successfully describes the unique feature of the combined EOF–PDF transport process: the decoupling of pressure and electrostatics, which is absent in the pure EOF study of [35]. From a practical standpoint, this pressure-tunable, pH-gated transport behaviour is directly relevant to the design of lab-on-a-chip diagnostic platforms, ion-selective biosensors, and nanofluidic energy-conversion devices, where an auxiliary pressure gradient could be used to fine-tune flow rate and reversal without compromising the chemically encoded ion selectivity of the channel.

Declarations

Conflict of interest

The authors declare that they have no conflict of interest.

Acknowledgments

The author thanks the Department of Mathematics and Computing Technology, National Institute of Technology Patna, for infrastructural support during the initial development of this work, and the Department of

Basic Science, School of Sciences, IIMT University, Meerut, for institutional support during its completion.

References

[1] Patrick Abgrall and Nam Trung Nguyen. Nanofluidic devices and their applications. *Analytical chemistry*, 80(7):2326–2341, 2008.

[2] Ashkan Babaie, Arman Sadeghi, and Mohammad Hassan Saidi. Combined electroosmotically and pressure driven flow of power-law fluids in a slit microchannel. *Journal of Non-Newtonian Fluid Mechanics*, 166(14-15):792–798, 2011.

[3] Naren Bag, S Bhattacharyya, Partha P Gopmandal, and H Ohshima. Electroosmotic flow reversal and ion selectivity in a soft nanochannel. *Colloid and Polymer Science*, 296(5):849–859, 2018.

[4] Aditya Bandopadhyay and Suman Chakraborty. Ionic size dependent electroosmosis in ion-selective microchannels and nanochannels. *Electrophoresis*, 34(15):2193–2198, 2013.

[5] RD Baños, JC Arcos, O Bautista, F Méndez, and EA Merchán-Cruz. Mass transport by an oscillatory electroosmotic flow of power-law fluids in hydrophobic slit microchannels. *Journal of the Brazilian Society of Mechanical Sciences and Engineering*, 43:1–15, 2021.

[6] Bhanuman Barman, Deepak Kumar, Partha P Gopmandal, and H Ohshima. Electrokinetic ion transport and fluid flow in a ph-regulated polymer-grafted nanochannel filled with power-law fluid. *Soft Matter*, 16(29):6862–6874, 2020.

[7] Laura Benson, Li-Hsien Yeh, Tzung-Han Chou, and Shizhi Qian. Field effect regulation of donnan potential and electrokinetic flow in a functionalized soft nanochannel. *Soft Matter*, 9(41):9767–9773, 2013.

[8] S Bhattacharyya, Z Zheng, and AT Conlisk. Electro-osmotic flow in two-dimensional charged micro- and nanochannels. *Journal of Fluid Mechanics*, 540:247–267, 2005.

[9] Somnath Bhattacharyya and Naren Bag. Enhanced electroosmotic flow of herschel-bulkley fluid in a channel patterned with periodically arranged slipping surfaces. *Physics of Fluids*, 31(7), 2019.

[10] Qianqian Cao and Hao You. Electroosmotic flow in mixed polymer brush-grafted nanochannels. *Polymers*, 8(12):438, 2016.

[11] Suman Chakraborty. Electroosmotically driven capillary transport of typical non-newtonian biofluids in rectangular microchannels. *Analytica Chimica Acta*, 605(2):175–184, 2007.

[12] Sourayon Chanda, Shayandev Sinha, and Siddhartha Das. Streaming potential and electroviscous effects in soft nanochannels: towards designing more efficient nanofluidic electrochemomechanical energy converters. *Soft Matter*, 10(38):7558–7568, 2014.

[13] Guang Chen and Siddhartha Das. Electroosmotic transport in polyelectrolyte-grafted nanochannels with ph-dependent charge density. *Journal of Applied Physics*, 117(18), 2015.

[14] Du-Soon Choi, Sungchan Yun, and WooSeok Choi. An exact solution for power-law fluids in a slit microchannel with different zeta potentials under electroosmotic forces. *Micromachines*, 9(10):504, 2018.

[15] Robert H Christopher and Stanley Middleman. Power-law flow through a packed tube. *Industrial & Engineering Chemistry Fundamentals*, 4(4):422–426, 1965.

[16] Siddhartha Das and Suman Chakraborty. Analytical solutions for velocity, temperature and concentration distribution in electroosmotic microchannel flows of a non-newtonian bio-fluid. *Analytica chimica acta*, 559(1):15–24, 2006.

[17] Alfredo De La Escosura-Muñiz and Arben Merkoçi. Nanochannels preparation and application in biosensing. *ACS nano*, 6(9):7556–7583, 2012.

[18] Shuyan Deng and Tan Xiao. Transient two-layer electroosmotic flow and heat transfer of power-law nanofluids in a microchannel. *Micromachines*, 13(3):405, 2022.

[19] Ranabir Dey, Tanmay Ghonge, and Suman Chakraborty. Steric-effect-induced alteration of thermal transport phenomenon for mixed electroosmotic and pressure driven flows through narrow confinements. *International Journal of Heat and Mass Transfer*, 56(1-2):251–262, 2013.

[20] Jan CT Eijkel and Albert van den Berg. Nanofluidics: what is it and what can we expect from it? *Microfluidics and Nanofluidics*, 1:249–267, 2005.

[21] Payam Fadaei, Hamid Niazmand, and Mohammad Amin Raoufi. Influence of finite size of ions on thermal transport of a simultaneous electrokinetic-pressure driven flow of power-law fluids in a slit microchannel. *Colloids and Surfaces A: Physicochemical and Engineering Aspects*, 634:127857, 2022.

[22] Daniel Figeys and Devanand Pinto. Lab-on-a-chip: a revolution in biological and medical sciences. 2000.

[23] Jun Gao, Wei Guo, Dan Feng, Huanting Wang, Dongyuan Zhao, and Lei Jiang. High-performance ionic diode membrane for salinity gradient power generation. *Journal of the American Chemical Society*, 136(35):12265–12272, 2014.

[24] Sandip Ghosal. Lubrication theory for electro-osmotic flow in a microfluidic channel of slowly varying cross-section and wall charge. *Journal of Fluid Mechanics*, 459:103–128, 2002.

[25] JL Harden, D Long, and A Ajdari. Influence of end-grafted polyelectrolytes on electro-osmosis along charged surfaces. *Langmuir*, 17(3):705–715, 2001.

[26] WH Herschel. Measurement of consistency of rubber-benzene solutions. *Kolloid-zeitschrift*, 39:291–298, 1926.

[27] RJ Hunter. Foundations of colloid science, 1987.

[28] Yong-jun Jian, Quan-sheng Liu, and Lian-gui Yang. Ac electroosmotic flow of generalized maxwell fluids in a rectangular microchannel. *Journal of Non-Newtonian Fluid Mechanics*, 166(21-22):1304–1314, 2011.

[29] Huan J Keh and Jau M Ding. Electrokinetic flow in a capillary with a charge-regulating surface polymer layer. *Journal of colloid and interface science*, 263(2):645–660, 2003.

[30] Dipankar Kundu, S Bhattacharyya, and Partha P Gopmandal. Ion partitioning and ion size effects on streaming field and energy conversion efficiency in a soft nanochannel. *Colloid and Polymer Science*, 300(9):1049–1062, 2022.

[31] Jun Li and Dongqing Li. Electroosmotic flow velocity in dna modified nanochannels. *Journal of colloid and interface science*, 553:31–39, 2019.

[32] Jin Liu, Moran Wang, Shiyi Chen, and Mark O Robbins. Molecular simulations of electroosmotic flows in rough nanochannels. *Journal of Computational Physics*, 229(20):7834–7847, 2010.

[33] Quansheng Liu, Yongjun Jian, and Liangui Yang. Alternating current electroosmotic flow of the jeffreys fluids through a slit microchannel. *Physics of fluids*, 23(10), 2011.

[34] Yongbo Liu and Yongjun Jian. The effects of finite ionic sizes and wall slip on entropy generation in electroosmotic flows in a soft nanochannel. *Journal of Heat Transfer*, 141(10):102401, 2019.

[35] Amit Malick. Electroosmotic transport of power-law fluids in zwitterionic soft nanochannels: effects of ion partitioning and ion steric. *The European Physical Journal Plus*, 141(6):719, 2026.

[36] Amit Malick and Bhanuman Barman. Electroosmotic flow modulation through soft nanochannel filled with power-law fluid under impacts of ion steric and ion partitioning effects. *Colloid Journal*, 86(4):610–626, 2024.

[37] Umberto Marini Bettolo Marconi, Michele Monteferrante, and Simone Melchionna. Electro-osmotic flow in coated nanocapillaries: a theoretical investigation. *Physical Chemistry Chemical Physics*, 16(46):25473–25482, 2014.

[38] Jacob H Masliyah and Subir Bhattacharjee. *Electrokinetic and colloid transport phenomena*. John Wiley & Sons, 2006.

[39] M Habibi Matin and H Ohshima. Thermal transport characteristics of combined electroosmotic and pressure driven flow in soft nanofluidics. *Journal of colloid and interface science*, 476:167–176, 2016.

[40] Meisam Habibi Matin and Hiroyuki Ohshima. Combined electroosmotically and pressure driven flow in soft nanofluidics. *Journal of colloid and interface science*, 460:361–369, 2015.

[41] D Mijatovic, Jan CT Eijkel, and Albert Van den Berg. Technologies for nanofluidic systems: top-down vs. bottom-up—a review. *Lab on a Chip*, 5(5):492–500, 2005.

[42] Zachary Milne, Li-Hsien Yeh, Tzung-Han Chou, and Shizhi Qian. Tunable donnan potential and electrokinetic flow in a biomimetic gated nanochannel with ph-regulated polyelectrolyte brushes. *The Journal of Physical Chemistry C*, 118(34):19806–19813, 2014.

[43] Michele Monteferrante, Simone Melchionna, Umberto Marini Bettolo Marconi, Marina Cretich, Marcella Chiari, and Laura Sola. Electroosmotic flow in polymer-coated slits: A joint experimental/simulation study. *Microfluidics and Nanofluidics*, 18:475–482, 2015.

[44] Rajorshi Paul, Debonil Maity, Pranshu Agrawal, Aditya Bandopadhyay, and Suman Chakraborty. Electrokinetics of non-newtonian fluids in poly-electrolyte grafted nanochannels: Effects of ion-partitioning and confinement. *Journal of Non-Newtonian Fluid Mechanics*, 283:104348, 2020.

[45] Sumita Pennathur and Juan G Santiago. Electrokinetic transport in nanochannels. 1. theory. *Analytical chemistry*, 77(21):6772–6781, 2005.

[46] Jeffrey L Perry and Satish G Kandlikar. Review of fabrication of nanochannels for single phase liquid flow. *Microfluidics and Nanofluidics*, 2:185–193, 2006.

[47] Aigars Piruska, Maojun Gong, Jonathan V Sweedler, and Paul W Bohn. Nanofluidics in chemical analysis. *Chemical Society Reviews*, 39(3):1060–1072, 2010.

[48] Antarip Poddar, Debonil Maity, Aditya Bandopadhyay, and Suman Chakraborty. Electrokinetics in polyelectrolyte grafted nanofluidic channels modulated by the ion partitioning effect. *Soft Matter*, 12(27):5968–5978, 2016.

[49] R Qiao and Narayana R Aluru. Ion concentrations and velocity profiles in nanochannel electroosmotic flows. *The Journal of chemical physics*, 118(10):4692–4701, 2003.

[50] Vijayaragavan Rajaram, Bharathi Varadharaj, and Prakash Jayavel. Impact of electroosmotic flow on a casson fluid driven by chemical reaction and convective boundary conditions. *Heat Transfer*, 50(5):4993–5019, 2021.

[51] Morteza Sadeghi, Mohammad Hassan Saidi, and Arman Sadeghi. Electroosmotic flow and ionic conductance in a ph-regulated rectangular nanochannel. *Physics of Fluids*, 29(6), 2017.

[52] Sandip Sarkar and Suvankar Ganguly. Fully developed thermal transport in combined pressure and electroosmotically driven flow of nanofluid in a microchannel under the effect of a magnetic field. *Microfluidics and Nanofluidics*, 18(4):623–636, 2015.

[53] Alessandro Siria, Philippe Poncharal, Anne-Laure Biance, Rémy Fulcrand, Xavier Blase, Stephen T Purcell, and Lydéric Bocquet. Giant osmotic energy conversion measured in a single transmembrane boron nitride nanotube. *Nature*, 494(7438):455–458, 2013.

[54] Howard A Stone, Abraham D Stroock, and Armand Ajdari. Engineering flows in small devices: microfluidics toward a lab-on-a-chip. *Annu. Rev. Fluid Mech.*, 36(1):381–411, 2004.

[55] Brian D Storey, Lee R Edwards, Mustafa Sabri Kilic, and Martin Z Bazant. Steric effects on ac electroosmosis in dilute electrolytes. *Physical Review E—Statistical, Nonlinear, and Soft Matter Physics*, 77(3):036317, 2008.

[56] Anthony Szymczyk, Haochen Zhu, and Béatrice Balannec. Pressure-driven ionic transport through nanochannels with inhomogenous charge distributions. *Langmuir*, 26(2):1214–1220, 2010.

[57] Eiichiro Tamaki, Akihide Hibara, Haeng-Boo Kim, Manabu Tokeshi, and Takehiko Kitamori. Pressure-driven flow control system for nanofluidic chemical process. *Journal of Chromatography A*, 1137(2):256–262, 2006.

[58] Shiojenn Tseng, Yu-Ming Li, Chih-Yuan Lin, and Jyh-Ping Hsu. Salinity gradient power: influences of temperature and nanopore size. *Nanoscale*, 8(4):2350–2357, 2016.

[59] Nadapana Vasu and Sirshendu De. Electroosmotic flow of power-law fluids at high zeta potentials. *Colloids and Surfaces A: Physicochemical and Engineering Aspects*, 368(1-3):44–52, 2010.

[60] Zehua Wang and Yongjun Jian. Heat transport of electrokinetic flow in slit soft nanochannels. *Micromachines*, 10(1):34, 2019.

[61] Jan H Wu and Huan J Keh. Diffusioosmosis and electroosmosis in a capillary slit with surface charge layers. *Colloids and Surfaces A: Physicochemical and Engineering Aspects*, 212(1):27–42, 2003.

[62] Jingnan Xing and Yongjun Jian. Steric effects on electroosmotic flow in soft nanochannels. *Meccanica*, 53:135–144, 2018.

[63] Song Xue, Li-Hsien Yeh, Yu Ma, and Shizhi Qian. Tunable streaming current in a ph-regulated nanochannel by a field effect transistor. *The Journal of Physical Chemistry C*, 118(12):6090–6099, 2014.

[64] Shulin Zeng, Chuan-Hua Chen, James C Mikkelsen Jr, and Juan G Santiago. Fabrication and characterization of electroosmotic micropumps. *Sensors and Actuators B: Chemical*, 79(2-3):107–114, 2001.

[65] ZhongQiang Zhang, HongWu Zhang, and HongFei Ye. Pressure-driven flow in parallel-plate nanochannels. *Applied Physics Letters*, 95(15), 2009.

[66] Cunlu Zhao and Chun Yang. Nonlinear smoluchowski velocity for electroosmosis of power-law fluids over a surface with arbitrary zeta potentials. *Electrophoresis*, 31(5):973–979, 2010.

[67] Cunlu Zhao, Emilijk Zholkovskij, Jacob H Masliyah, and Chun Yang. Analysis of electroosmotic flow of power-law fluids in a slit microchannel. *Journal of colloid and interface science*, 326(2):503–510, 2008.

[68] Guangpu Zhao and Yongjun Jian. Thermal transport of combined electroosmotically and pressure driven nanofluid flow in soft nanochannels. *Journal of Thermal Analysis and Calorimetry*, 135:379–391, 2019.

[69] Jiaxuan Zheng and Yongjun Jian. Space electroosmotic thrusters in ion partitioning soft nanochannels. *Micromachines*, 12(7):777, 2021.

[70] WB Zimmerman, JM Rees, and TJ Craven. Rheometry of non-newtonian electrokinetic flow in a microchannel t-junction. *Microfluidics and Nanofluidics*, 2:481–492, 2006.